inventions

MDPI

Article

Feasibility Study of the CO_2 Regenerator Parameters for Oxy-Fuel Combustion Power Cycle

Vladimir Kindra *, Ivan Komarov, Sergey Osipov, Olga Zlyvko and Igor Maksimov

Department of Innovative Technologies of High-Tech Industries, National Research University "Moscow Power Engineering Institute", 111250 Moscow, Russia; komarovii@mpei.ru (I.K.); osipovsk@mpei.ru (S.O.); zlyvkoov@mpei.ru (O.Z.); maksimovia98@gmail.com (I.M.)

* Correspondence: kindra.vladimir@yandex.ru

Abstract: The atmosphere carbon dioxide content grows subsequently due to anthropogenic factors. It may be considerably mitigated by the development of thermal power plants with near zero emissions. A promising way is the transition to the semi-closed oxy-fuel combustion power cycles with carbon dioxide and water vapor mixture as a working fluid. However, their wide implementation requires reduction of the metal consumption for the highly efficient regeneration system. This paper discloses the results of feasibility study for the regeneration system of the prospective oxy-fuel combustion power plant. The effect of operating parameters on the cycle energy efficiency, overall dimensions, and the cost of the regenerator was determined. Underheating increase in the regenerator by 1 °C leads to the net efficiency factor drop of the oxy-fuel combustion power cycle by 0.13% at average and increases fuel costs by 0.28%. Increase of pressure drop in the hot channel by 1% leads to efficiency drop by 0.14%. The optimum set of design and operating parameters of the feed heating system has been determined, which ensures the best technical and economic indicators of electrical power generation: the minimum cumulative costs are achieved when underheating in the regenerator is 20 °C and pressure drop in the hot channel is 4%, under the use of S-shaped fins channels.

Keywords: thermodynamic cycle; heat exchanger; hydraulic loss; heat transfer surface; energy efficiency

Citation: Kindra, V.; Komarov, I.; Osipov, S.; Zlyvko, O.; Maksimov, I. Feasibility Study of the CO_2 Regenerator Parameters for Oxy-Fuel Combustion Power Cycle. *Inventions* **2022**, *7*, 66. https://doi.org/10.3390/inventions7030066

Academic Editors: Umberto Lucia, Debora Fino, Giulia Grisolia and Shyy Woei Chang

Received: 6 July 2022
Accepted: 26 July 2022
Published: 29 July 2022

1. Introduction

1.1. Low-Carbon Power Production

Nowadays hydrocarbon fuels are the main sources for the electricity production, which results in emission of a remarkable amount of greenhouse gases. This accelerates the global warming effect, which is a threat to sustainable development [1]. Therefore, remarkable efforts are directed to the emission level mitigation. New technical solutions in the zero carbon power generation may become the main driver for the "Green economics".

Existing thermal power plants successfully mitigate such toxic emissions as nitrogen oxides and sulfur [2,3]. On the contrary, a lot of the carbon dioxide is produced with organic fuel combustion and prevention of its emission is still a difficult problem. Despite the fact that many methods for the CO_2 capture are known, their wide introduction is limited by the rapid increase of produced electricity price [4]. This is due to the carbon dioxide low partial pressure in flue gases.

It determines prospects for oxy-fuel combustion in electric power production. Specific feature of this technology is the hydrocarbon fuel combustion in the pure oxygen environment that produces carbon dioxide and water vapor (Figure 1) [5]. The combustion product content simplifies the separation of carbon dioxide and water vapor with

minimal power consumptions by the vapor condensing. This reduces price of the greenhouse gas capturing, which makes prerequisites for cheaper and environmentally friendly power facilities.

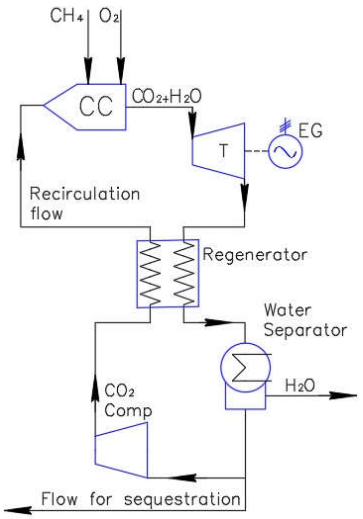

Figure 1. Heat flow chart of a semi-closed cycle with oxy-fuel combustion.

There are many power production cycles based on oxy-fuel combustion. The following are widely known: the semi-closed oxy-fuel combustion combined cycle (SCOC-CC), the MATIANT cycles, the Allam cycle, the Graz cycles, the CES cycle, and the membrane technology cycles (AZEP, ZEITMOP) [6]. In addition, technologies of oxy-fuel combustion are known and have been tested in pulverized-fuel fired boilers [7,8] and also in circulating fluidized-bed boilers [9,10].

The first modifications of these power facilities appeared at the end of the 20th century, and today the USA, Japan, and EU countries are actively developing this direction. Research studies are being carried out, test facilities are being built, and foundations for the zero emission pilot facilities are being created using grant funding, active "green technology" backing, and through the creation of legislation bases. Large power corporations cooperate in a buildup of demonstration facilities with power outputs of up to 50 MW [11].

Among the oxy-fuel combustion power cycles, the Allam cycle is one of the most prospective. The main advantages of this cycle are the zero greenhouse gas emission and high efficiency. At the initial temperature 1100 °C, the cycle net efficiency may be above 50% [12].

1.2. Oxy-Fuel Combustion Technology Challenge

This high efficiency is due to the advanced regeneration system that remarkably reduces the cold source heat losses [13]. The regenerator is one of the key cycle components. Its efficiency directly determines the power production facility efficiency. High regeneration degree and efficiency of the cycle heat exchanging equipment are top important aspects of design and development of the oxy-fuel combustion power plants.

The regeneration degree may be increased only by reduction of the regenerator final underheating. This will directly influence the heat exchanger dimensions and its total price. The regenerator price may comprise above 10% of the facility main equipment price, therefore the regeneration system parameters directly determine the electricity production price and the power production block return rate [14,15].

Regenerator is a key element of cycle that operates at high temperature and pressure. The working fluid temperature may be above 660 °C and the pressure difference between

the hot and cold parts may be up to 27 MPa. This determines the necessity of structural solutions that will provide reliable equipment operation at these operation parameters combined with the high compactness [16].

The PCHE heat exchangers by Heatric have shown themselves for operation in carbon dioxide cycles due to the capability to operate at high temperature and pressure drop. In these devices, the channels are formed in plates by photo-chemical etching and the plates are connected by diffusion welding [17]. The heat exchanging surfaces are usually semicircle channels etched in plates but the heat exchange effectiveness in these devices is not high.

1.3. Thermal-Hydraulic Characteristics for PCHE Heat Exchangers

Many methods are known for improvement of the heat transfer in semicircle section channels. For example, the computer simulation analysis allowed detailed studies of heat exchange in zigzag channels with different flow turn angles [18]. Changes of the heat carrier flow path may cause changes of the heat flow intensity and the hydraulic performance, first of all of the device pressure losses.

One more geometry parameter that remarkably influences the channel flow performance is the channel cross-section shape. Paper [19] shows that the flow in rectangular cross-section channel has rather low heat release resistance. The hydraulic losses in this type channels are remarkable. It confirms that the channel shape is determined not only by the manufacturing technology and labor input, but also by the specific features of the thermohydraulic process.

Channel manufacturing in plates by chemical etching allows the heat exchange surface configuration that is complicated or impossible by standard technology. This opens wide possibilities for application of different heat exchange intensifiers including the complicated shaped ones.

Many researchers pay attention to the optimization of heat exchanger geometry; the heat exchange surfaces are arrays of flow turbulators. One of the promising areas for improvement of PCHE surfaces design is the use of turbulators made with NACA airfoil profile or its modifications. Thus, the proceedings [20,21] show the results of experimental and numerical studies of the channels with airfoil fins of different shapes. The intensifier geometry being determined by its dimensions and profile directly affects heat transfer intensity and the level of gas-dynamic losses. The main characteristic feature which makes the use of the channels with airfoil fins promising is a significantly lower level of gas-dynamic resistance as compared to zigzag channels, while heat transfer intensity in these channels is worse. In work [22], proceeding establishes that the most technically and economically valuable set of design parameters of the channel with airfoil fins field is determined also by consumption parameters of the heat exchanger.

Papers [23–25] present results of development and test of channels with S-shaped fin intensifiers. The specific channel shape and geometry result in the heat transfer level similar to the zigzag channel one but with times smaller pressure losses.

The use of different types of heat exchange intensifiers leads to a change in thermal and gas-dynamic characteristics of the flow in the heat exchanger channel. Choice of the heat exchanging surface shape for a regenerative system is a multi-criteria problem. It is necessary to take into account the intensifier shape influence upon the thermal performance, Nusselt criteria, specific heat flow, etc., combined with the influence upon the channel hydraulic resistance. Both the factors directly influence the heat exchanger equipment size. The complicated shape channel manufacturing content also determines the heat exchanger manufacturing expenses.

The Allam cycle facilities have high power production efficiency. The compromise between this efficiency and the main heat exchanging equipment price is a special problem.

This paper summarizes results of design and parameters studies of a regenerative system for the oxy-fuel combustion power cycle. The analysis determines the optimal set of parameters that provide minimal total expenses.

2. Materials and Methods

2.1. Heat Balance of the Allam Cycle

This investigation concentrates on the Allam cycle (Figure 2) regeneration system. The facility installed power is 200 MW.

The classic Allam cycle scheme assumes the regenerator as a multi-flow heat exchanger. This system is thermodynamically efficient but it cannot work in practice.

In this work, the regenerative system consists of two double flow heat exchangers. In the first, the turbine exhaust gas gives its heat to the combustor inlet flow. In the second, the heated air from the air separation unit meets the CO_2 flow supplied to the turbine cooling. The first heat exchanger power is an order higher than the second one, therefore this work discloses verifying of the first heat exchanger operation parameters.

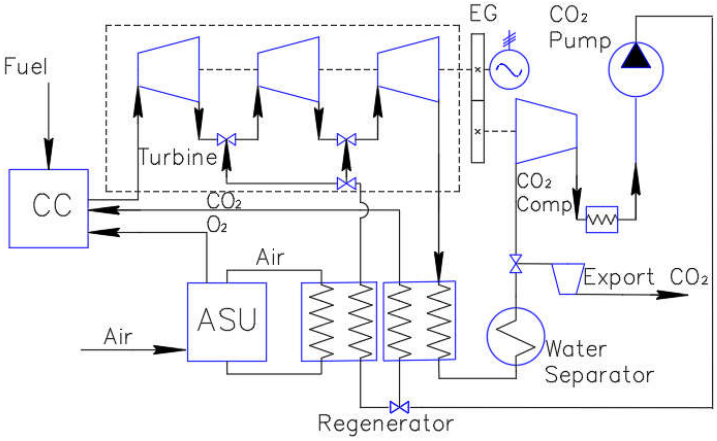

Figure 2. Allam cycle with two heat exchanger regeneration scheme.

The heat flow and thermodynamic process analysis corresponded to the method [26] and employed the S/W code Aspen Plus and the thermophysical parameters database NIST REFPROP. Table 1 shows key parameters of the Allam cycle heat balance simulation.

Table 1. Parameters of the Allam cycle heat balance simulation.

Parameter	Value
CO_2 turbine inlet temperature, °C	1100
CO_2 turbine inlet pressure, MPa	30
CO_2 turbine outlet pressure, MPa	3
CO_2 turbine coolant temperature, °C	200
Multi-stage intercooled compressor massflow, kg/s	600
Isentropic efficiency of turbines and compressors, %	90
Pumps isentropic efficiency, %	75
Mechanical efficiency of turbines, compressors, pumps, power generator %	99
Power generator and electric motor efficiency, %	99
Cooler-separator exit working fluid temperature, °C	55
Minimum working fluid temperature, °C	30
ASU power, MW	31

The mathematical model of the Allam cycle prepared in Aspen Plus software package is shown in Figure 3. Oxygen from the air separation unit is compressed in the cooled oxygen compressor and delivered to the combustion chamber. Heat transferred from the compressor is usefully utilized in the carbon dioxide-based Rankine cycle. Natural gas is compressed and delivered to the combustion chamber under the pressure of 30 MPa, where carbon dioxide and water are generated as a result of combustion. Combustion products with the temperature of 1100 °C are expanded in the cooled gas turbine, thereafter residual heat is given to cold flow of CO_2 in the waste heat exchanger. The service medium is cooled in the separator feed cooler, thereafter moisture is removed from the cycle, and a part of a carbon dioxide flow is sampled for disposal. The rest of the flow goes to recycling: it is partially compressed in the cooled compressor and cooled prior to compression in the carbon dioxide pump. After compression, a part of the flow is sampled for cooling down of the gas turbine, and the main flow is heated in the waste heat exchanger and delivered to the combustion chamber. The cycle is closed.

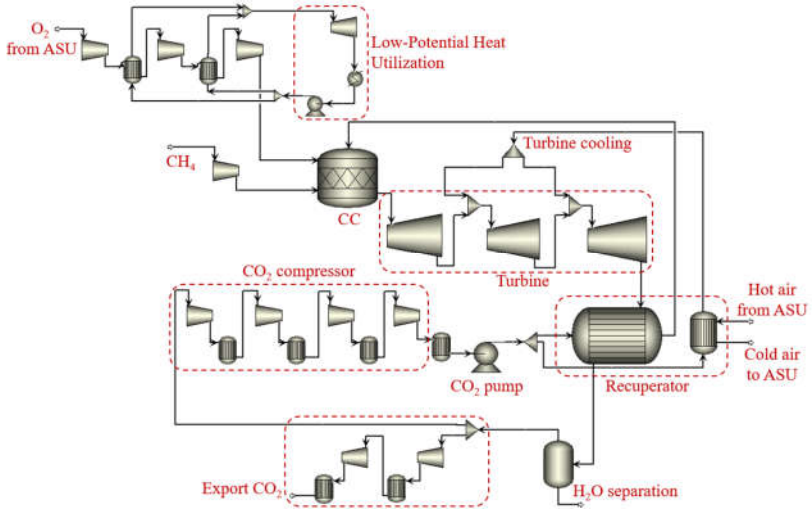

Figure 3. The mathematical model of the Allam cycle in Aspen Plus.

Processes of expansion and compression in turbo-machines are calculated with constant isentropic efficiency according to the equations shown below.

For expansion process in the turbine:

$$h_2 = h_1 - (h_1 - h_2') \cdot \eta_{oi.T}, \quad (1)$$

where h_1 and h_2 are specific enthalpies of the medium before and after the process of pressure variation, kJ/kg;

$h_{2'}$—a specific enthalpy of the medium caused by isentropic pressure variation, kJ/kg;

$\eta_{oi.T}$—isentropic turbine efficiency.

For compression process in the compressor:

$$h_2 = h_1 + (h_2' - h_1)/\eta_{oi.C}, \quad (2)$$

where $\eta_{oi.C}$—isentropic compressor efficiency.

The mathematical model of the surface heat exchanger is based on solution of the heat balance equation:

$$G_1 \cdot (h_{11} - h_{12}) = G_2 \cdot (h_{22} - h_{21}) = Q, \quad (3)$$

where h_{11} and h_{21} are specific enthalpies of hot and cold flows at the heat exchanger inlet, kJ/kg;

h_{12} and h_{22}—specific enthalpies of hot and cold flows at the heat exchanger outlet, kJ/kg;

G_1 and G_2—flow rates of hot and cold heat-transfer media, kg/s.

Q—the heat exchanger thermal capacity, kW;

The power unit net efficiency factor is calculated by the following equation:

$$\eta_{net} = \frac{N_{net}}{B \cdot LHV}, \quad (4)$$

where N_{net}—the power unit net electrical capacity, MW;

B—fuel flow rate, kg/s;

LHV—low heating value of natural gas, MJ/kg.

The power unit net electrical capacity is determined as follows:

$$N_{net} = \left(N_{CO2.T} \cdot \eta_m \cdot \eta_g + N_{LPHU}\right) - \left(\frac{N_{O2.C} + N_{CO2.C} + N_{CO2.P} + N_{fuel.C} + N_{ex.C}}{\eta_m \cdot \eta_{mot}} + N_{ASU}\right), \quad (5)$$

where $N_{CO2.T}$—the carbon dioxide turbine capacity, MW;

η_m and η_g—mechanical efficiency factor and efficiency factor of the power generator;

N_{LPHU}—the low-grade heat utilization capacity, MW;

$N_{O2.C}$, $N_{CO2.C}$, $N_{fuel.C}$, $N_{CO2.P}$ $N_{ex.C}$—capacities of oxygen, carbon dioxide and fuel compressors, carbon dioxide pump and disposal compressor, MW;

η_{mot}—the electrical motor efficiency;

N_{ASU}—power consumed by the air separation unit, MW.

The unit of AKAr-40/35 grade is reviewed as an ASU with an input for generation of 1 m^3 of oxygen equal to 0.714 kWh/m^3 and the maximum output of 3400 m^3/h.

2.2. Heat Exchange Equipment

The present proceeding reviews PCHE apparatuses with few versions of heat exchange surface design (Figure 4) as a regenerator: straight semicircular channels (Figure 4a), zigzag semicircular channels (Figure 4b), with S-shaped fins (Figure 4c), and airfoil fins (Figure 4d). As of this date they are one of the most studied (numerically and experimentally) channel shapes for PCHE. The geometric parameters of channels are presented in Table 2.

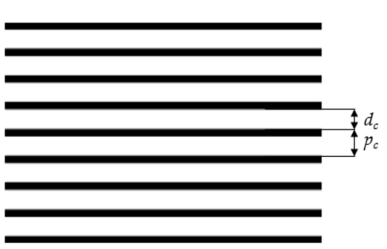

(**a**)

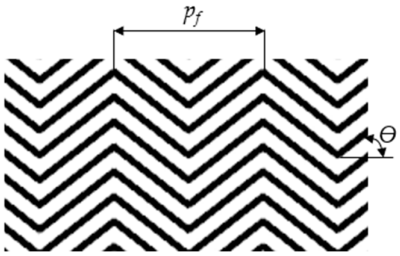

(**b**)

(**c**) (**d**)

Figure 4. Considered configurations of heat exchanging surfaces. (**a**) straight semicircular channels, (b) zigzag semicircular channels, (**c**) with S-shaped fins, and (**d**) airfoil fins.

Table 2. Channels geometry parameters.

Parameter	Value
Plate thickness, mm	1.5
Plate width, mm	600
Semi-circular	
Channel pitch p_c, mm	2.4
Channel diameter d_c, mm	2
Zigzag channel	
Channel angle θ, °	52
Channel pitch, mm	2.4
Channel diameter, mm	2
Channel step, mm	7.565
Airfoil fins	
Fin depth, mm	0.94
Pin pitch on the x-axis L, mm	8
Pin pitch on the y-axis H, mm	2.2
Fin length l, mm	4
Fin width h, mm	0.8
Fin profile	NACA0020
S-shape	
Fin pitch p_x, mm	7.565
Fin depth, mm	0.94
Hydraulic diameter, mm	1.09

As of this date multiple different approaches for design calculation of heat exchangers have been developed. Methods based on calculation of log mean temperature difference (LMTD methods), on calculation of effectiveness and the number of transfer units (ε-NTU methods), and others are known. Recently special attention is drawn to issues of the artificial intelligence use for calculation and analysis of thermal characteristics of heat exchangers [27,28] and also for optimization of their design parameters [29–31]. Due to the fact that the service medium in the regenerator is a mixture of carbon dioxide and vapors, and temperatures and thermophysical properties of service media change significantly during heat transfer process [32], special attention should be drawn to local changes of characteristics during calculation and optimization of the apparatus design.

Structural analysis of the regenerator was carried out by the segmental split method. The device length is split into elements (Figure 5). In each element, the performance, the main heat transfer parameters, and hydraulic losses are calculated. On the contrary, to the

mean-logarithmic head LMTD method, this method discloses local working fluid parameters and may take into account non-linear temperature distribution along the channel and the existing pinch-points [33].

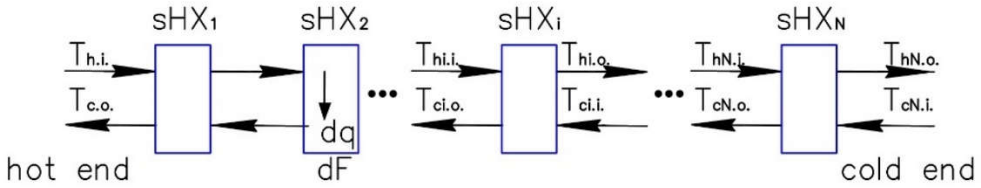

Figure 5. Scheme of regenerator split.

The results of thermodynamic analysis of heat balance are used for design calculation of the Allam cycle regenerator. Table 3 shows the basic operating parameters of the regenerator.

Table 3. Regenerator working parameters.

Parameters	Hot Channel	Cold Channel
CO_2 temperature at the unit inlet, °C	665	60
CO_2 temperature at the unit exit, °C (varies)	75	652
Fluid massflow, kg/s	637	543
Fluid pressure, MPa	3	30
Molar moisture content in the CO_2 flow, %	6.9	0.6
Heat power, MW (varies)	462	

Heat balance for each segment looks as follows:

$$\Delta Q_i = G_h \Delta h_{h.i} = G_c(h_{ci.o} - h_{ci.i}), \quad (6)$$

where ΔQ_i is a heat flow in the elementary segment, W;

G_h, G_c—cumulative flow rates of hot and cold heat-transfer media, kg/s;

$\Delta h_{h.i}$—hot fluid specific enthalpy variation in ith segment, J/kg;

$h_{ci.i}$ and $h_{ci.o}$—specific enthalpies of the hot medium at inlet and outlet of ith segment, J/kg;

The required heat exchange area of a segment is determined as follows:

$$\Delta F_i = \frac{\Delta Q_i}{k \Delta T}, \quad (7)$$

where k—the segment heat transfer coefficient, W/(m^2 °C), which is determined by the following equation:

$$\frac{1}{k} = \frac{1}{\alpha_h} + \frac{t_w}{\lambda_w} + \frac{1}{\alpha_c}, \quad (8)$$

where α_h and α_c—heat exchange coefficients in hot and cold channels, W/(m^2 °C);

t_w—a metal wall thickness, m;

λ_w—a metal thermal conductivity coefficient, W/(m °C);

ΔT—temperature difference in a segment, °C.

The heat exchange coefficient in the channel directly depends on the flow mode in the channel and on configuration of heat exchange surfaces. Analysis of the channel flow thermal and hydraulic parameters employs semi-empirical correlation equations for Nusselt criteria Nu and the hydraulic losses coefficient f. In the semicircle section channel, Nu may be accurately calculated by Gnielinski correlation [34]:

$$Nu = \frac{\alpha d_h}{\lambda_f} = \frac{\frac{f}{8}(Re - 1000)Pr}{1 + 12.7(Pr^{2/3} - 1)\sqrt{\frac{f}{8}}}, \quad (9)$$

where Re—Reynolds criteria in the channel;
λ_f—fluid thermal conductivity, W/(m °C);
Pr—Prandtl criteria;
f—Moody friction factor, defined as:

$$f = \left(\frac{1}{1.8logRe - 1.5}\right)^2. \quad (10)$$

The Reynolds criteria in the channel is determined as:

$$Re = \frac{wd_h}{\nu}, \quad (11)$$

where w—heat carrier flow velocity (varies), m/s,
ν—kinematic viscosity coefficient, m²/s,
d_h—character dimension, m, determined as:

$$d_h = \frac{4F}{P} = \frac{\pi d_c^2}{4\left(\pi\frac{d_c}{2} + d_c\right)}, \quad (12)$$

where F—channel flow path area, m²;
P—contact perimeter, m;
d_c—semicircle diameter, m.
The flow velocity in the channel is determined from the continuity equation:

$$w = \frac{G}{\rho A}, \quad (13)$$

where ρ—fluid density, kg/m³;
A—channel flow area, m².
The linear hydraulic losses coefficient for the semicircle section channel is calculated by Colebrook–White equation:

$$f = \frac{1}{\left[2\lg\left(\frac{2.51}{Re\sqrt{f}} + \frac{\Delta}{3.7}\right)\right]^2}, \quad (14)$$

where Δ—relative roughness.
The following correlation equations are known for the zigzag channel (52° turn angle) with a semicircular cross-section, which have been obtained as a result of experimental studies [21]:

$$Nu = 0.1696Re^{0.629}Pr^{0.317}, \quad (15)$$

$$f = 0.1924Re^{-0.091}. \quad (16)$$

The same paper presents correlation equations for channels with S-shaped fins:

$$Nu = 0.174Re^{0.593}Pr^{0.43}, \quad (17)$$

$$f = 0.4545Re^{-0.340}. \quad (18)$$

In [22], for channels with airfoil fins, the following equations are proposed for the Nusselt number and loss factor:

$$Nu = 0.02671Re^{0.8}Pr^{0.3}(h/H)^{-0.09177}(l/L)^{-0.01118}, \quad (19)$$

$$f = 0.05754Re^{-0.1923}(h/H)^{-0.2264}(l/L)^{-0.03108}. \quad (20)$$

where h and l—fins width and length, m;

H and L—transverse and longitudinal spacing fins, m.

In all equations, it is assumed that the fluid performance determining temperature is the segment mean temperature.

As heat exchange intensity and pressure drops in the regenerator are determined by the heat transfer medium flow rate in channels, this parameter is variable. Figure 6 shows an algorithm of design calculation of the Allam cycle regenerator PCHE.

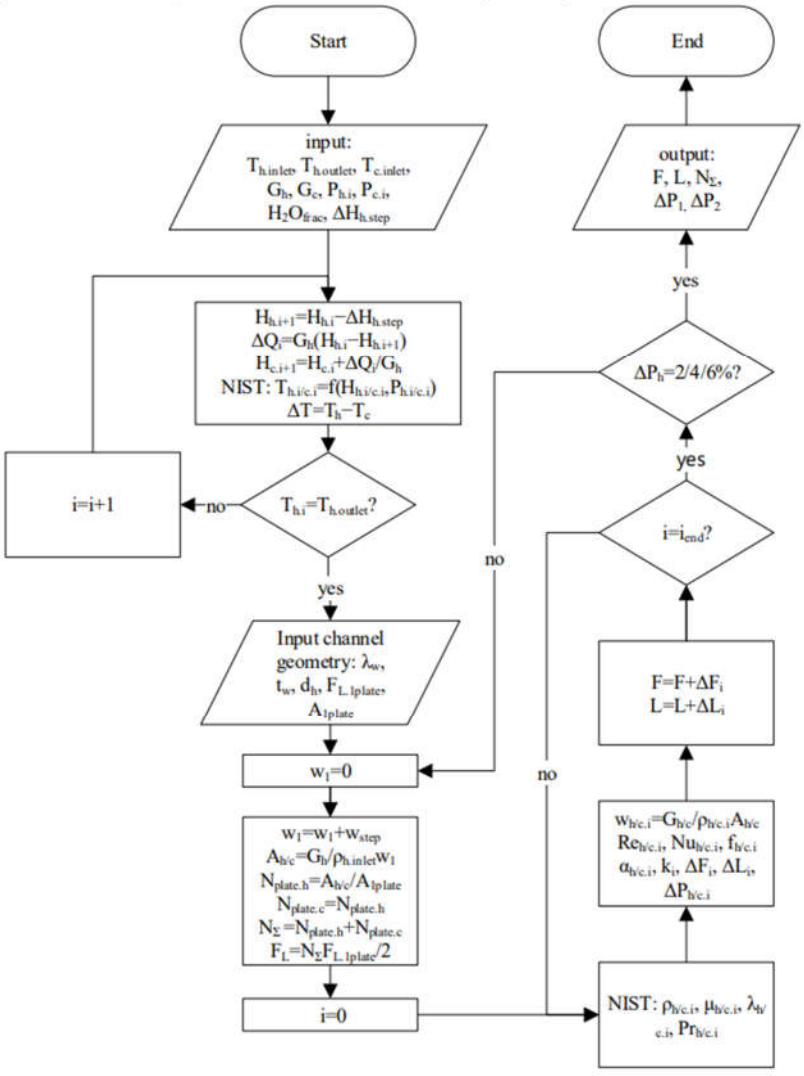

Figure 6. Algorithm for the design calculation of the regenerator.

The regenerator operates at high temperature, therefore its heat exchanging surfaces materials must meet specific requirements. At temperatures above 550 °C, nickel alloys such as Inconel 617 that have high heat strength and resistance are required [35]. At lower working parameters, it is possible to use high carbon steels such as SS316. With respect to these features, the regenerator is made of two parts, the hot made of Inconel 617 and the cool of SS316.

2.3. Methodology of Feasibility Study

In this work, the regenerator optimization goal is determination of the operation parameters and heat exchanging surface type that provides minimal total expenses on the main stages of the power plant lifecycle.

One of the main indicators used for assessment of cost efficiency of electrical power generation is Levelized Cost of Energy (LCOE). The use of this indicator as a target function of optimization studies requires detailed study of all power unit equipment cost, expenses for its maintenance, personnel, etc.

The regeneration system changes are assumed to influence only the cycle efficiency and do not require remarkable structure changes of other equipment. It is also assumed that changes in parameters of the feed heating system do not result in changes of administrative costs. Therefore, it is possible to assume that changes of the total expenses will be determined only by the heat exchanger equipment and fuel expenses. This assumption allows performing technical and economic optimization of the feed heating system without analyzing the cost of other power unit equipment and avoid usage of LCOE as a target function.

Thus, the optimization target function is the total expenses increment that is defined as a sum of increment of the fuel expenses caused by changes of the cycle efficiency and increment of the regeneration system expenses caused by the change of heat exchange equipment price:

$$\delta C_{summ} = \delta C_{fuel} + \delta C_{HE} \rightarrow \min \quad (21)$$

where δC_{summ}—total increment of the expenses, RuR/year;

δC_{fuel}—increment of the fuel expenses, RuR/year;

δC_{HE}—increment of the annual expenses for heat exchange equipment, RuR/year.

Annual expenses for the heat exchange equipment are determined as a total value of the apparatus divided by its entire service life.

Expenses for the fuel spent on the electric power production may be calculated as:

$$C_{fuel} = \frac{3600 \cdot N \cdot h \cdot C_{gas}}{\eta \cdot Q}, \quad (22)$$

where N—block net power, MW,

h—estimated operation time, hr/year,

C_{gas}—natural gas fuel price, RuR/m^3;

Q—fuel lower heating value, MJ/m^3;

η—block net efficiency.

The power plant efficiency directly depends upon the cycle regeneration rate, because the high cycle efficiency is provided by the heat transition from the turbine exhaust flow to the cold flow supplied to the combustor [36]. The second important parameter that influences the production efficiency is the heat exchanging equipment pressure losses that determine the additional energy spent on the working fluid compression and circulation.

Increase of the regeneration rate by reduction of the regenerator underheating reduces the mean integral temperature head, which requires larger heat exchanging area. The necessary heat exchange area depends upon the heat exchange level in the device channels. This allows the conclusion on the final heat exchange area to be determined by the necessary underheating level dT and the acceptable pressure losses in channels dP:

$$F_{HE} = f(dT, dP). \quad (23)$$

The final heat exchanger price directly depends upon the material expenses that are determined by the heat exchanger area and upon the surface configuration and manufacturing complexity.

Thus, the increase of regenerator temperature head causes two effects. It increases the fuel expenses caused by the lower cycle thermal efficiency and reduces the heat exchanger equipment final price. Changes of the acceptable heat exchanger pressure losses cause similar effects. On the other side, changes of the heat exchange surface configuration including the intensifier placement, may cause not only reduction of the device dimensions and price.

Thus, optimization of the main structural and operating parameters may be split into the following stages:

1. The Allam cycle heat flow analysis, calculation of the basic operation parameters of the regeneration system;
2. Structural analysis of the heat exchanging device based on the heat flow analysis of different heat exchanger configurations;
3. Analysis of the regenerator underheating and pressure losses influence upon the facility efficiency and the fuel expenses;
4. Analysis of the regenerator underheating and acceptable pressure losses influence upon the regenerator dimensions and price;
5. Summarizing fuel and regenerator manufacturing expenses, comparison with the basic version, determination of the nest parameters.

The regenerator price assessment is based on the expenses sensitivity method [37]. This sensitivity method assumes the product market price equal to the product creation and selling expenses (Table 4). The final device price is calculated as the sum of all heat exchanger elements prices that depend upon the metal consumption and the manufacturing procedures.

Table 4. Constant values assumed for the regenerator price calculation.

Parameter	Value
Fuel price, RuR/m^3	5.67
Block annual operation, hr	6000
Low heating value, MJ/m^3	35.59
Regenerator estimated life, years	20
Plate photo-chemical etching, RuR/m^2 (1$ = 70 RuR)	11,900
Inconel 617 price, RuR/kg	10,500
SS316 price, RuR/kg	1400

The regenerator price assessment involves the following assumptions:

1. Channel manufacturing by photo-chemical etching has constant price per an area unit;
2. The nonproductive expenses, taxes, administrative expenses, etc., are taken into account by a multiplying coefficient $k = 1.45$;
3. The fuel natural gas price is assumed as the mean whole sale Russian power production industry price.

3. Results and Discussion

3.1. The Cycle Thermodynamic Analysis

Figure 7a shows the results of thermodynamic analysis and parameters in the main units of the Allam cycle, and Figure 7b shows the cycle T-S diagram. In case of underheating in the regenerator equal to 15 °C and 1% of pressure drop in the heat exchanger, the cycle net efficiency factor is 47.45%.

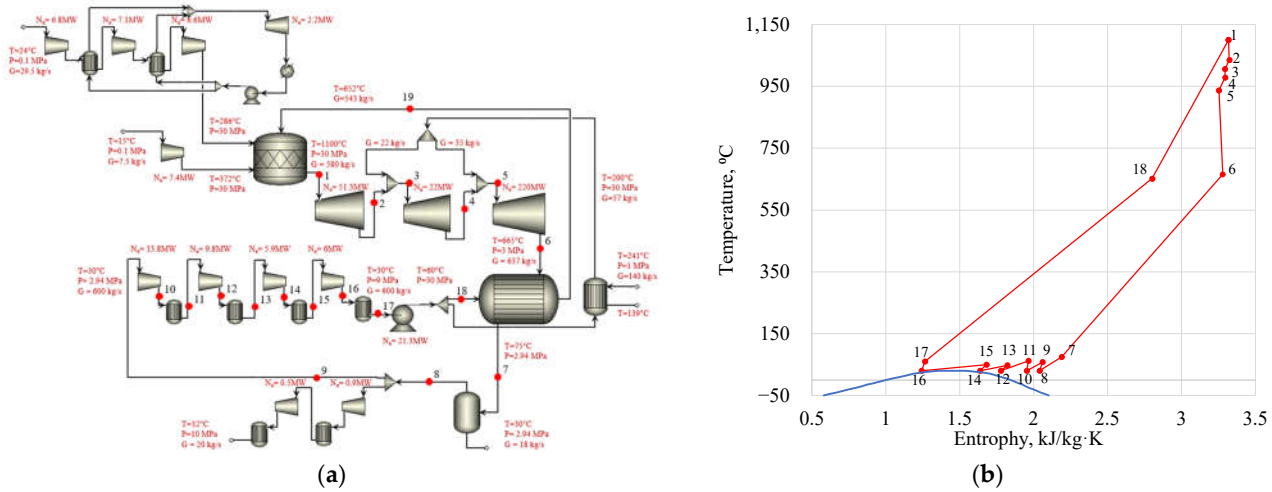

Figure 7. Calculation results of the Allam cycle heat balance: (**a**) parameters in the main units; (**b**) T-S diagram.

The Allam cycle energy efficiency indicators vary widely in the existing proceedings. In particular, different assessments are given for the cycle net efficiency factor—from 40 to 58% [5,11,38]. It is determined by the initial parameters of the cycle, choice of the air separation unit model, availability and type of the carbon dioxide turbine cooling model, the regenerator model and an approach to determination of the service medium thermophysical properties.

The base case of the feed heating system assumes underheating to be equal to 15 °C, and the hot channel pressure drop—1%. This set of parameters allows ensuring comparatively high energy efficiency indicator; however, the analysis of heat exchange equipment overall dimensions and cost is required for this case.

3.2. The Design Parameters of the Regenerator

In the regenerative system the working fluid is a mixture of carbon dioxide and water vapor that is produced by the hydrocarbon fluid combustion. When the heat carrier flow is cooled below a definite level the vapor condenses, which results in non-linear temperature distribution along the channel (Figure 8a). This causes appearance if a pinch-point, which introduces limits on the acceptable temperature head and increases the required heat exchange surface area. Therefore, the minimal underheating on the cold end cannot be below 12.5 °C. In this case, the minimal temperature difference in the pinch-point will be about 0.5 °C. Heat transfer at this temperature head will require a remarkable heat exchange area (Figure 8b).

The heat exchanger consists of two sections made of different materials, the high temperature section of Inconel 617 that operates above 550 °C and the low temperature section of SS316 carbon steel. At the underheat of 12.5 °C, less than 17% of the total heat exchange surface is the high temperature section that is mostly caused by a remarkable steel consumption for the heat exchange provision in the low temperature head section.

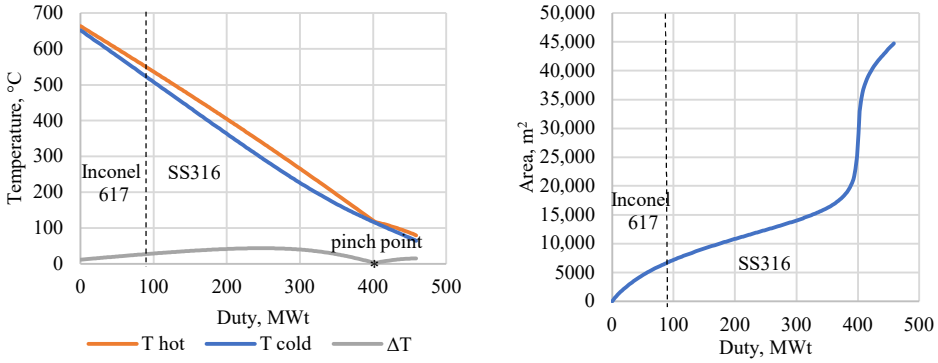

Figure 8. Regenerator diagram: (**a**) T-Q diagram; (**b**) area-duty diagram.

This results in a remarkable increase of the heat exchanger dimensions at reduction of the underheating level. When the underheating drops down from 17.0 °C to 12.5 °C, the heat exchange area grows more than twice (Figure 9a). At further reduction, it is obvious that because of the indefinitely small pinch-point temperature difference, there will be needed an indefinitely large area to provide the heat exchange. It will directly influence the device price.

Increase of the heat carrier flow velocity may be a method for the dimensions reduction. Higher heat transfer from the heat exchange surfaces and the thermal resistance reduction require smaller heat transfer area but on the other side it causes larger hydraulic losses in the channels (Figure 9b). Another method for reduction of the regenerator dimensions is change of the heat exchange surface configuration and application of intensifiers. The plots show that transition from straight semicircular channels to more complicated shapes is accompanied by reduction of the required heat exchange area. Thus, under pressure drop of 1% and underheating of 15 °C, heat exchange area in the apparatus with zigzag channels is 1.78 times less than in case with straight channels, with airfoil fins—1.89 times, and with S-shaped fins—1.91 times. Meanwhile as allowable pressure drops increase, the use of airfoil fins becomes more advantageous.

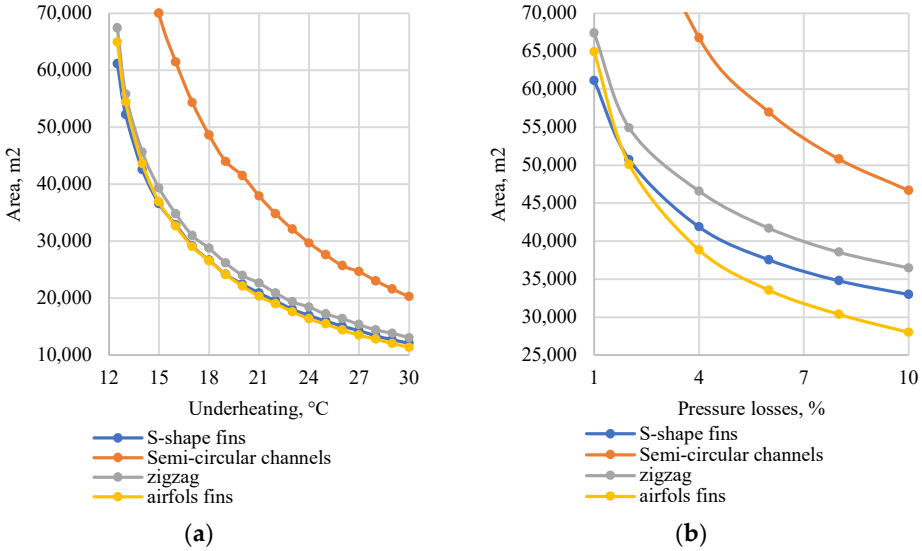

Figure 9. Dependence of heat transfer area from: (**a**) underheating, (**b**) regenerator pressure losses.

Configuration of heat exchange surfaces influences the thermal and hydrodynamic processes in the channels. At equal initial flow velocities, the device with S-shape intensifiers shows higher heat transfer level (Figure 10a) than the device with semicircle channels, therefore it requires smaller heat transfer area. Together with this, the pressure losses in channels are smaller because of the shorter flow path (Figure 10b).

Changes in heat transfer parameters along the flow path are worth of a special attention. Heat transfer coefficient in a hot channel is remarkably higher than in a cold one because of different heat carrier flow velocities, in the hot and cold ends the velocities differ 5 and 10 times respectively (Figure 10c). Together with this, a velocity drop is seen in both the channels by reaching the cold end that is caused by the flow density drops. Changes in the heat carrier thermal-physical parameters, especially of the heat conductivity, are also taken into account. At 30 MPa pressure, subsequent cooling of CO_2 mixture with water shows a non-linear change in its performance (Figure 10d).

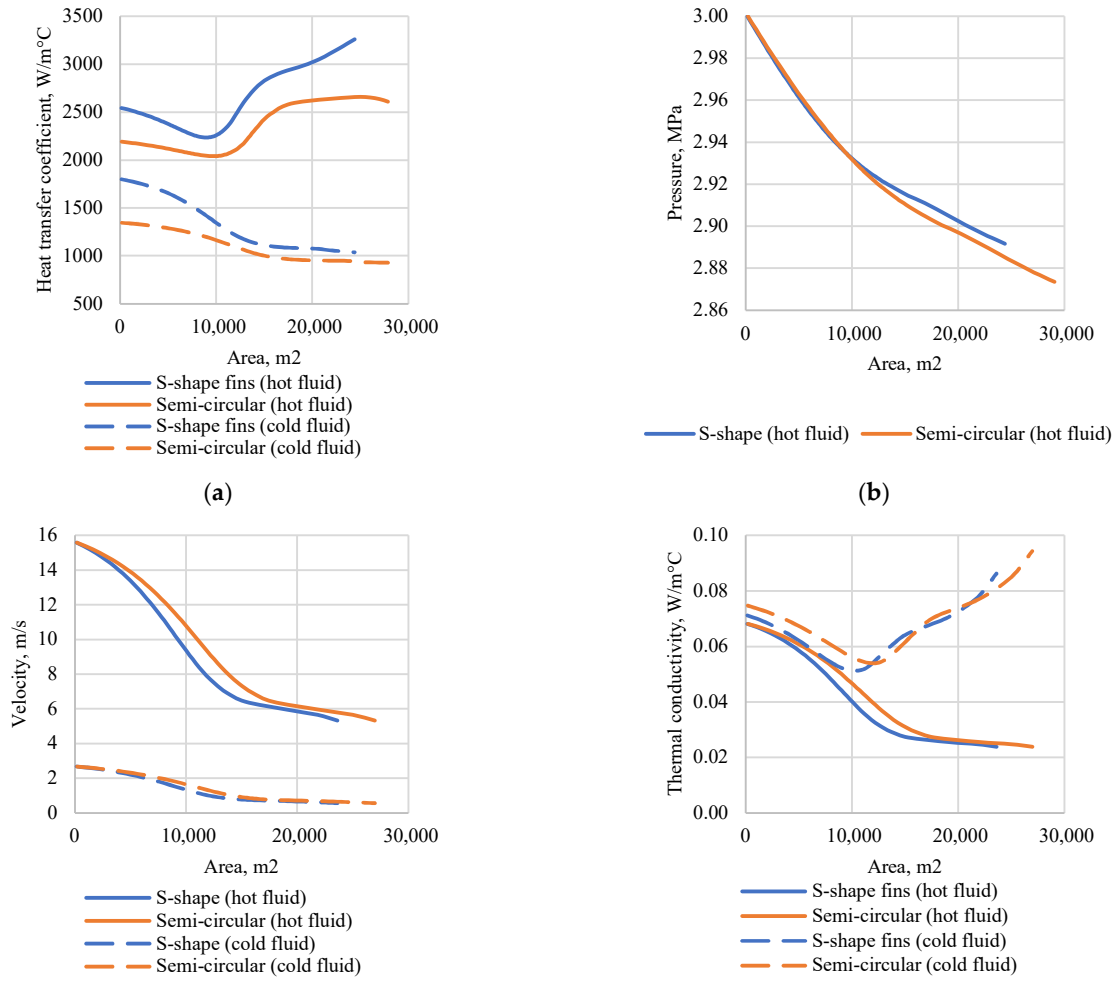

Figure 10. Distributions at hot flow velocity 5 m/s of: (**a**) heat transfer coefficient, (**b**) regenerator pressure losses; (**c**) fluid velocity; (**d**) thermal conductivity.

Thus, the heat transfer surface choice and the heat transfer intensification must include analysis of heat exchange and hydrodynamics. Application of the channels with improved thermal and hydraulic efficiency allows investment reduction by the dimensions reduction, but the larger manufacturing labor of these channels must be taken into account.

The regenerator manufacturing expenses are mostly determined by the metal consumption and remarkably depend upon the operating parameters (Figure 11). In a regenerator with semicircle channels and hot channel pressure losses of 1%, an increase in underheating from 12.5 °C to 17.0 °C reduces expenses 2.3 times from 391 to 166 million RuR/year. Therefore, the operating parameters choice must take into account the regeneration system expenses.

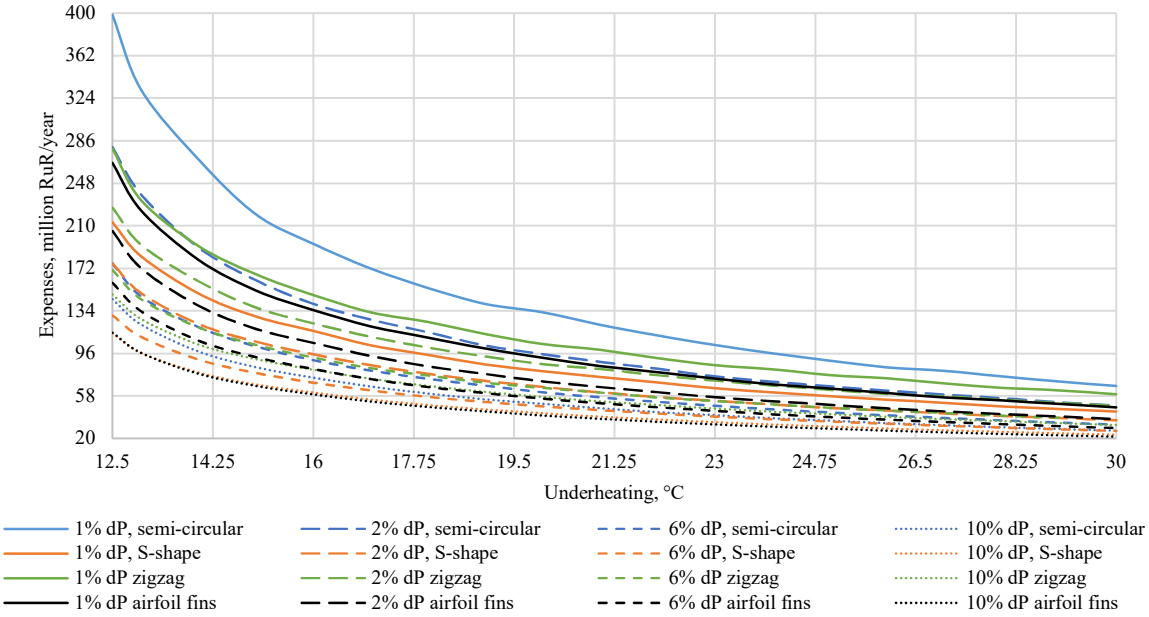

Figure 11. Regenerative system expenses vs. underheating and pressure losses.

3.3. Change in the Energy Efficiency of the Power Facility

An advanced regeneration system provides high production efficiency that makes a favorable effect upon the fuel expenses. Figure 12 shows the regenerator underheating influence upon the cycle efficiency (Figure 12a) and fuel expenses (Figure 12b). A 1 °C increase of temperature difference reduces the cycle efficiency by 0.13% and the fuel expenses grow 4 million RuR/year. Due to the higher heat losses in the cold source, the regenerator allows using turbine exhaust heat. Higher regenerator pressure losses also reduce the cycle efficiency. At the hot channel pressure losses of 1%, the electricity production efficiency drops down by 0.14%.

Thus, as underheating in the feed heating system increases from 12.5 °C to 20 °C under pressure drop of 1%, the cycle net efficiency factor drops from 47.7% to 46.8%, and as pressure drop increases from 1% to 10% with underheating of 12.5 °C, it drops to 46.38%.

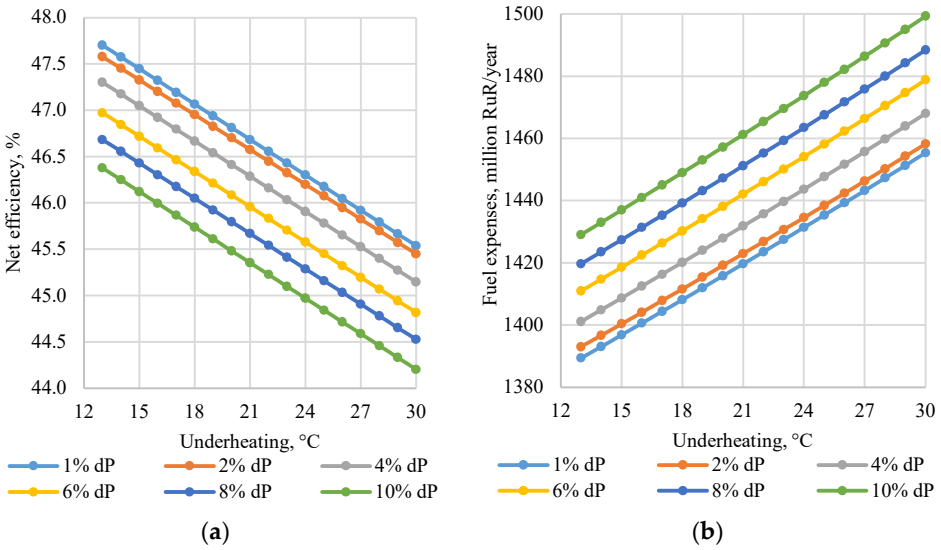

Figure 12. Underheating vs.: (**a**) net efficiency, (**b**) fuel expenses.

3.4. Optimization of Design Parameters of the Regenerator

The two opposite effects create an extremum of the total expenses function. The extremum is located between two limiting cases, the case of maximal cycle net efficiency and the indefinitely large regenerator size and the case of low efficiency and low price of the regeneration system. Figure 13 shows dependencies of the total expenses from the underheating and pressure losses. The analysis includes changes of fuel expenses caused by the regenerator parameters change. The analysis base is the regenerator with semicircle channels, 15 °C underheating, and the hot channel pressure losses of 4%.

Channels geometry directly determines both costs for the feed heating system and the scope of its optimum operating parameters. Thus, while the maximum increment of costs equals to 32 mln. RuR/year for semicircular channels has been achieved under 23 °C underheating and 4% pressure drop, in case of zigzag channels the same set of parameters being optimum leads to increment of costs equal to 29.8 mln. RuR/year. The maximum increment of costs for channels with airfoil fins as compared to the base level is achieved under 21 °C underheating and 4% pressure drop and amounts to 45.75 mln. RuR/year.

The plot shows that the maximal expenses reduction is seen in the regenerator with S-shape intensifier, 20 °C underheating, and pressure losses of 4% of the inlet pressure. In this case, the expenses are 46.83 million RuR/year smaller than the base version.

Thus, the Allam cycle facility with an effective regeneration system has an optimal set of operation parameters that provides minimal expenses concerned to the regeneration system.

It is worth mentioning that the regenerator shows optimal hot channel pressure losses of 4% of the inlet pressure. These parameters provide a balance between the regenerator size and the additional power losses in the carbon dioxide pump. The optimal underheating directly depends upon the heat exchange surface configuration and the assumed acceptable level of pressure losses so the optimization of the regenerator design and operating parameters is a multi-criteria problem. It requires analysis of different relations between the financial performance of the power facility.

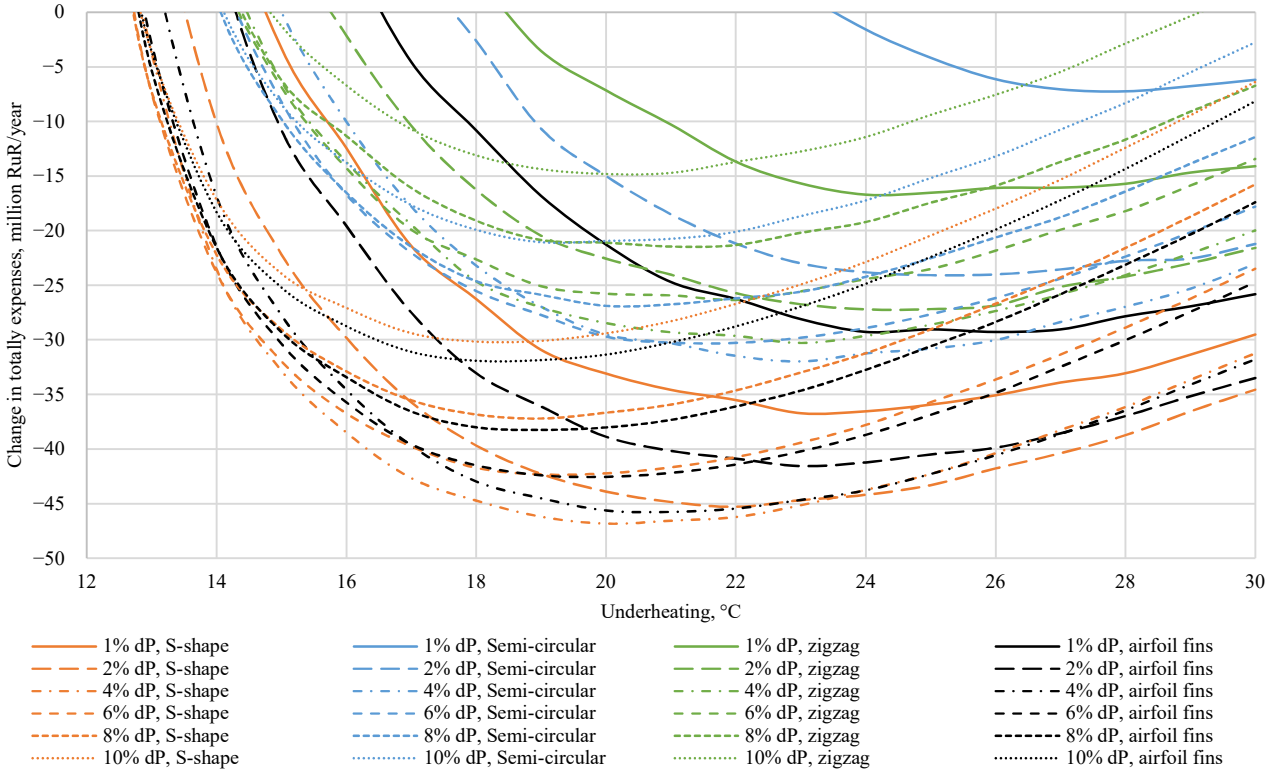

Figure 13. Total expenses on the regeneration system vs. underheating and pressure losses.

4. Conclusions

The present proceeding has shown and tested the algorithm of technical and economic analysis of the feed heating system operation for the power unit operated according to the Allam cycle, and also has provided recommendations for selection of its operating and design parameters. Efficiency of the use of PCHE regenerators with different shapes of channels have been compared, namely: straight semicircular, zigzag, with S-shaped fins and airfoil fins. The proceeding concludes that:

1. Underheating increase in the feed heating system by 1 °C leading to efficiency factor drop of the net Allam cycle by an average of 0.13% and increases fuel costs by 0.28%. Increase of pressure drop in the hot channel by 1% reduces efficiency of electrical power generation by an average of 0.14%.
2. Increase of underheating in the regenerator from 12.5 °C to 15 °C results in reduction of the required heat exchange area by an average of 42.5%, from 15 °C to 20 °C—by 40%, and from 20 °C to 25 °C—by 30.5%, for the channels of all shapes under review.
3. Transition from straight semicircular channels to more complicated shapes is accompanied by a reduction of the required heat exchange area: under pressure drop of 1% and underheating of 15 °C, heat exchange area in the apparatus with zigzag channels is 1.78 times less than in case with straight channels, with airfoil fins—1.89 times, and with S-shaped fins—1.91 times. Meanwhile the most cost-efficient set of geometric parameters of the regenerator is determined by operating parameters of the apparatus.
4. The maximum increment of cumulative costs is achieved under underheating and pressure drop equal to 23 °C and 4%—for straight semicircular channels (−32 mln. RuR/year as compared to the base level), 23 °C and 4% – for zigzag channels (−29.8 mln. RuR/year), 20 °C and 4%—for channels with airfoil fins (−45.75 mln. RuR/year), and 21 °C and 4%—for channels with S-shaped fins (−46.83 mln. RuR/year).

Author Contributions: Conceptualization, V.K. and I.K.; methodology, V.K.; software, I.M.; validation, I.M., S.O. and O.Z.; formal analysis, O.Z.; investigation, I.M.; resources, S.O.; data curation, I.K. and S.O.; writing—original draft preparation, V.K.; writing—review and editing, O.Z.; visualization, I.M.; supervision, V.K.; project administration, I.K.; funding acquisition, I.K. All authors have read and agreed to the published version of the manuscript.

Funding: This study conducted by the Moscow Power Engineering Institute was financially supported by the Ministry of Science and Higher Education of the Russian Federation (project no. FSWF-2020-0020).

Data Availability Statement: Not applicable.

Conflicts of Interest: The authors declare no conflict of interest.

References

1. Change, Intergovernmental Panel on Climate. "Climate change 2007: The physical science basis." *Agenda* **2007**, *6*, 333.
2. Dutka, M.; Ditaranto, M.; Løvås, T. Application of a central composite design for the study of NOx emission performance of a low NOx burner. *Energies* **2015**, *8*, 3606–3627.
3. Volchyn, I.; Haponych, L. Estimate of the sulfur dioxide concentration at thermal power plants fired by Donetsk coal. *Power Technol. Eng.* **2014**, *48*, 218–221.
4. Adu, E.; Zhang, Y.; Liu, D.; Tontiwachwuthikul, P. Parametric process design and economic analysis of post-combustion CO2 capture and compression for coal-and natural gas-fired power plants. *Energies* **2020**, *13*, 2519.
5. Rogalev, A.; Rogalev, N.; Kindra, V.; Komarov, I.; Zlyvko, O. Research and Development of the Oxy-Fuel Combustion Power Cycles with CO2 Recirculation. *Energies* **2021**, *14*, 2927.
6. IEAGHG *Oxy-Combustion Turbine Power Plants*; International Energy Agency Greenhouse Gas: Cheltenham, UK, 2015.
7. Chen, L.; Yong, S.Z.; Ghoniem, A.F. Oxy-fuel combustion of pulverized coal: Characterization, fundamentals, stabilization and CFD modeling. *Prog. Energy Combust. Sci.* **2012**, *38*, 156–214.
8. Shaddix, C.R.; Molina, A. Particle imaging of ignition and devolatilization of pulverized coal during oxy-fuel combustion. *Proc. Combust. Inst.* **2009**, *32*, 2091–2098.
9. Leckner, B.; Gómez-Barea, A. Oxy-fuel combustion in circulating fluidized bed boilers. *Appl. Energy* **2014**, *125*, 308–318.
10. Czakiert, T.; Bis, Z.; Muskala, W.; Nowak, W. Fuel conversion from oxy-fuel combustion in a circulating fluidized bed. *Fuel Processing Technol.* **2006**, *87*, 531–538.
11. Allam, R.; Martin, S.; Forrest, B.; Fetvedt, J.; Lu, X.; Freed, D.; Brown Jr, G.W.; Sasaki, T.; Itoh, M.; Manning, J. Demonstration of the Allam Cycle: An update on the development status of a high efficiency supercritical carbon dioxide power process employing full carbon capture. *Energy Procedia* **2017**, *114*, 5948–5966.
12. Rogalev, A.; Rogalev, N.; Kindra, V.; Zlyvko, O.; Vegera, A. A Study of Low-Potential Heat Utilization Methods for Oxy-Fuel Combustion Power Cycles. *Energies* **2021**, *14*, 3364.
13. Penkuhn, M.; Tsatsaronis, G. Exergy analysis of the Allam cycle. In Proceedings of the 5th international symposium–supercritical CO_2 power cycles, San Antonio, Texas, 28–31 March 2016; pp. 6–7.
14. Chaturvedi, R.; Kennedy, E.; Metew, S. CO_2 Sequestration by Allam Cycle. 2021. Available online: https://repository.upenn.edu/cbe_sdr/135/ (accessed on 1 July 2022).
15. Kindra, V.; Rogalev, A.; Lisin, E.; Osipov, S.; Zlyvko, O. Techno-economic analysis of the oxy-fuel combustion power cycles with near-zero emissions. *Energies* **2021**, *14*, 5358.
16. Hesselgreaves, J.E.; Law, R.; Reay, D. *Compact Heat Exchangers: Selection, Design and Operation*; Butterworth-Heinemann: Oxford, UK, 2016.
17. Diffusion Bonded Heat Exchangers and Support | Heatric. Available online: https://www.heatric.com (accessed on 27 may 2022).
18. Aneesh, A.; Sharma, A.; Srivastava, A.; Chaudhury, P. Effects of wavy channel configurations on thermal-hydraulic characteristics of Printed Circuit Heat Exchanger (PCHE). *Int. J. Heat Mass Transf.* **2018**, *118*, 304–315.
19. Lee, S.-M.; Kim, K.-Y. Comparative study on performance of a zigzag printed circuit heat exchanger with various channel shapes and configurations. *Heat Mass Transf.* **2013**, *49*, 1021–1028.
20. Chen, F.; Zhang, L.; Huai, X.; Li, J.; Zhang, H.; Liu, Z. Comprehensive performance comparison of airfoil fin PCHEs with NACA 00XX series airfoil. *Nucl. Eng. Des.* **2017**, *315*, 42–50.
21. Xu, X.; Ma, T.; Li, L.; Zeng, M.; Chen, Y.; Huang, Y.; Wang, Q. Optimization of fin arrangement and channel configuration in an airfoil fin PCHE for supercritical CO_2 cycle. *Appl. Therm. Eng.* **2014**, *70*, 867–875.
22. Kwon, J.G.; Kim, T.H.; Park, H.S.; Cha, J.E.; Kim, M.H. Optimization of airfoil-type PCHE for the recuperator of small scale brayton cycle by cost-based objective function. *Nucl. Eng. Des.* **2016**, *298*, 192–200.
23. Ngo, T.L.; Kato, Y.; Nikitin, K.; Tsuzuki, N. New printed circuit heat exchanger with S-shaped fins for hot water supplier. *Exp. Therm. Fluid Sci.* **2006**, *30*, 811–819.
24. Ngo, T.L.; Kato, Y.; Nikitin, K.; Ishizuka, T. Heat transfer and pressure drop correlations of microchannel heat exchangers with S-shaped and zigzag fins for carbon dioxide cycles. *Exp. Therm. Fluid Sci.* **2007**, *32*, 560–570.

25. Nikitin, K.; Kato, Y.; Ishizuka, T. Experimental thermal-hydraulics comparison of microchannel heat exchangers with zigzag channels and S-shaped fins for gas turbine reactors. In Proceedings of the of Fifteenth International Conference on Nuclear Engineering, Nagoya, Japan, 22–26 April 2007; pp. 22–26.
26. Rogalev, A.; Kindra, V.; Komarov, I.; Osipov, S.; Zlyvko, O. Structural and Parametric Optimization of S-CO2 Thermal Power Plants with a Pulverized Coal-Fired Boiler Operating in Russia. *Energies* **2021**, *14*, 7136.
27. Sridharan, M. Applications of artificial intelligence techniques in heat exchanger systems. In *Advanced Analytic and Control Techniques for Thermal Systems with Heat Exchangers*; Elsevier: Amsterdam, The Netherlands, 2020; pp. 325–334.
28. Sridharan, M. Application of fuzzy logic expert system in predicting cold and hot fluid outlet temperature of counter-flow double-pipe heat exchanger. In *Advanced Analytic and Control Techniques for Thermal Systems with Heat Exchangers*; Elsevier: Amsterdam, The Netherlands, 2020; pp. 307–323.
29. Krzywanski, J. A general approach in optimization of heat exchangers by bio-inspired artificial intelligence methods. *Energies* **2019**, *12*, 4441.
30. Xie, G.; Sundén, B.; Wang, Q. Optimization of compact heat exchangers by a genetic algorithm. *Appl. Therm. Eng.* **2008**, *28*, 895–906.
31. Krzywanski, J. Heat transfer performance in a superheater of an industrial CFBC using fuzzy logic-based methods. *Entropy* **2019**, *21*, 919.
32. Krasnoshchekov, E.; Kuraeva, I.; Protopopov, V. Local heat transfer of carbon dioxide at supercritical pressure under cooling conditions. *High Temp.* **1969**, *7*, 856.
33. Lu, M.; Yan, X.; Wang, J.; Sun, Y.; Gong, Z. Thermal hydraulic performance analysis of PCHE precooler for supercritical CO_2 Brayton cycle. In Proceedings of the 2019 5th International Conference on Transportation Information and Safety (ICTIS), Liverpool, UK, 14–17 July 2019; pp. 537–541.
34. Çengel, Y.A. *Heat and Mass Transfer: A Practical Approach*; McGraw-Hill: New York, USA, 2007.
35. Hosseini, H.S.; Shamanian, M.; Kermanpur, A. Characterization of microstructures and mechanical properties of Inconel 617/310 stainless steel dissimilar welds. *Mater. Charact.* **2011**, *62*, 425–431.
36. Rogalev, N.; Kindra, V.; Komarov, I.; Osipov, S.; Zlyvko, O.; Lvov, D. Comparative Analysis of Low-Grade Heat Utilization Methods for Thermal Power Plants with Back-Pressure Steam Turbines. *Energies* **2021**, *14*, 8519.
37. Caputo, A.C.; Pelagagge, P.M.; Salini, P. Heat exchanger design based on economic optimisation. *Appl. Therm. Eng.* **2008**, *28*, 1151–1159.
38. Scaccabarozzi, R.; Gatti, M.; Martelli, E. Thermodynamic analysis and numerical optimization of the NET Power oxy-combustion cycle. *Appl. Energy* **2016**, *178*, 505–526.